Appl Phys B (2010) 101: 649–659
DOI 10.1007/s00340-010-4183-7

Applied Physics B
Lasers and Optics

QEPAS for chemical analysis of multi-component gas mixtures

A.A. Kosterev · L. Dong · D. Thomazy · F.K. Tittel · S. Overby

Received: 27 May 2010 / Revised version: 20 July 2010 / Published online: 15 September 2010

Abstract A gas sensor based on quartz-enhanced photoacoustic spectroscopy and using near-infrared, fiber-coupled diode lasers as an excitation source was developed for chemical analysis of gas mixtures containing H_2S, CO_2, and CH_4 at concentrations from 0 to 100%. Analysis of physical phenomena affecting the sensor operation is performed, the sensor performance is evaluated, and simple algorithms are developed to derive concentrations of the gases from detected electrical signals.

1 Introduction

Quartz-enhanced photoacoustic spectroscopy (QEPAS) is a gas-sensing technique that features an absorption detection module with dimensions of 1–2 cm and allows the analysis of gas samples of a few mm^3 in volume [1–5]. This technique is based on the use of a quartz tuning fork (QTF) as a detector for acoustic oscillations induced in an absorbing gas by modulated optical radiation. The QTF is a piezo-electric element which converts its deformation into separation of electrical charges. Due to its geometry and arrangement of the film electrodes deposited on the quartz crystal, the QTF is selectively sensitive to the sound originating in a small, 100–300 μm wide, space between its prongs. This property determines the simplest configuration of the QEPAS absorption detection module (spectrophone) shown in Fig. 1a. The force acting on the QTF prongs is created by pressure difference in the cylindrical acoustic wave produced in the gas by the modulated laser radiation. Thus, the QTF is effectively probing absorption in the optical path equal to its thickness, typically ∼0.3 mm. The minimum detectable absorption coefficient achieved with such a short path length is often insufficient for practical needs. Therefore, in most reported QEPAS based gas sensors a spectrophone configuration shown in Fig. 1b was used. In addition to the QTF, it contains two pieces of rigid tubing placed along the excitation laser beam and positioned close to, but not touching, the QTF, with 30–50 μm gaps. These tubes form a so-called microresonator, which concentrates the acoustic pressure and, when properly designed, provides an additional resonant acoustic enhancement [6]. The sensitivity to absorption coefficient in configuration from Fig. 1b is up to 30 times higher than in configuration shown in Fig. 1a.

Design parameters and performance of the Fig. 1b spectrophone are dependent on the properties of the gas where it is immersed, in particular, the gas density and the speed of sound. Besides, QEPAS detection sensitivity can be affected by the dynamics of molecular relaxation, namely, the energy transfer rate from the optically excited state to translational motion of gas molecules. This rate can change with the carrier gas. Most of the QEPAS sensors reported to date were intended for monitoring a concentration of one or several trace chemical species in the otherwise invariable carrier gas. The examples include measuring pollutants in ambient air [7, 8] or physiological markers in human breath [9]. However, there is a wide range of applications where the bulk composition of the carrier gas can change. One such application, which was an immediate motivation for this work, is monitoring H_2S concentration in the gas diffusing through the fluid isolation layer of the flexible oil risers. Flexible oil risers are multilayer pipes for transporting oil,

A.A. Kosterev · L. Dong · D. Thomazy · F.K. Tittel (✉)
Electrical and Computer Engineering Department,
Rice University, 6100 Main St., Houston, TX 77005, USA
e-mail: fkt@rice.edu

S. Overby
NKT Flexibles I/S, Priorparken 510, 2605 Broendby, Denmark

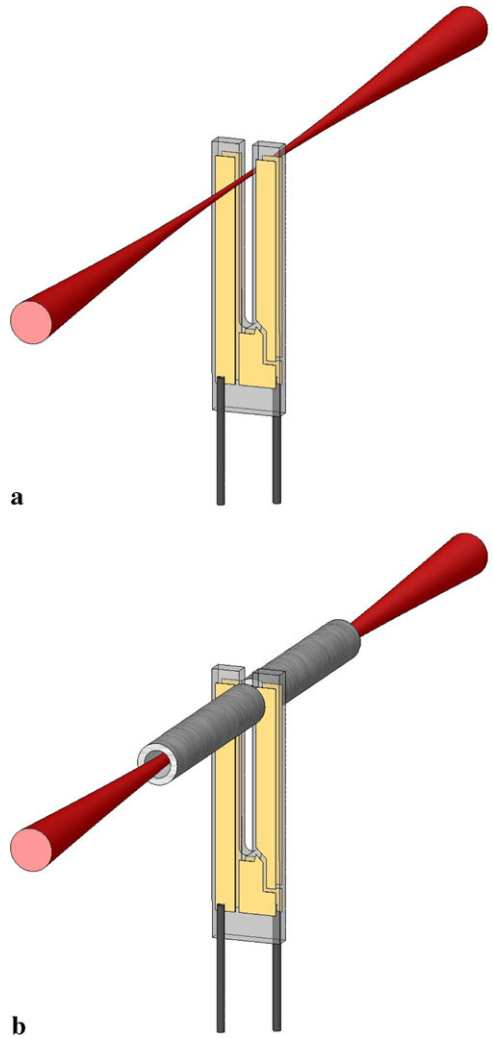

Fig. 1 Schematic representation of two kinds of spectrophones

most often from undersea sources to floating platforms. Hot oil is kept inside by a layer of plastic (fluid isolation layer), while the outer metal layers provide the structural stability. The corrosion rate of the metal elements strongly depends on the composition of the surrounding gas, and in particular, concentration of H_2S at the 100–1000 parts-per-million by volume (ppm) level. The gas environment of the metal layers is formed by the species diffusing from oil through the fluid isolation layer, and is composed mostly of CO_2 and CH_4, varying from almost pure carbon dioxide to almost pure methane.

In this paper we present a QEPAS based gas sensor for analyzing composition of a model gas mixture consisting of CO_2, CH_4 and trace amounts of H_2S. All the measurements were carried out at atmospheric pressure, as required by the application. Using experimental results, we develop algorithms of deriving concentrations of the analytes from the measured signals, as well as general approaches to applying QEPAS for chemical analysis of gases with variable bulk composition.

2 Sensor design

The general principles and configuration of a QEPAS based gas-sensing platform for quantifying one chemical species have been described previously [2]. For this work, the sensor system was modified to allow sequential detection of three different species, H_2S, CO_2, and CH_4 (Fig. 2). This was done in a similar way as reported in [12]. Near-infrared (overtone) absorption bands were selected to permit the use of reliable and convenient diode lasers developed for telecommunication needs. The CO_2 and H_2S NIR absorption bands overlap, and therefore one DFB DL (DL1 in Fig. 2) at $\lambda = 1.58$ μm was used for the detection of both species. This laser delivered ∼38 mW, measured after the spectrophone. A second laser, DL2 with $\lambda = 1.65$ μm, was used to detect CH_4. The optical power of this laser measured after the spectrophone was 16.0 mW. Fiber couplers were utilized to split the radiation of each laser and direct 99% of the optical power to one of the two spectrophones, and send the remaining fraction of radiation to reference cells. Permanently sealed reference cells contained high concentrations of the target species to ensure optical absorption in the 1–5% range. For CO_2 and H_2S we used long reference cells with optical path length $l = 16.5$ cm. The CH_4 reference cell was shorter, with $l = 2.5$ cm. Each cell incorporated a pre-aligned, fixed fiber collimator and a photodiode. During the concentration measurements the laser wavelength was locked to the selected absorption line using a 3f component of the photodiode signal as an error signal in a DC laser current regulation loop.

One of the QEPAS spectrophones (Sp1) used only a QTF as shown in Fig. 1a. Its design is presented in Fig. 3a. The QTF was mounted in the center of a cylindrical cell ∼16 mm high with inner diameter 13 mm, equipped with tilted AR coated windows and gas connectors. The QTF crystal was precisely positioned using a specially designed alignment jig, eliminating the need of active optical alignment. The laser radiation from a single-mode optical fiber was first collimated and then focused between the prongs of the QTF. The optical elements and the QTF were passively aligned using precisely machined components. A polyethylene foam sheet ∼1 mm thick was placed around the inner cell walls to suppress acoustic resonances of the cell itself.

The second spectrophone (Sp2) incorporated a microresonator as shown in Fig. 1b. A photograph of the identical module with the top hermetic lid removed is shown in Fig. 3b. This module was fabricated by Achray Photonics Inc. based on our instructions. Active optical alignment was used to ensure free propagation of the radiation through the

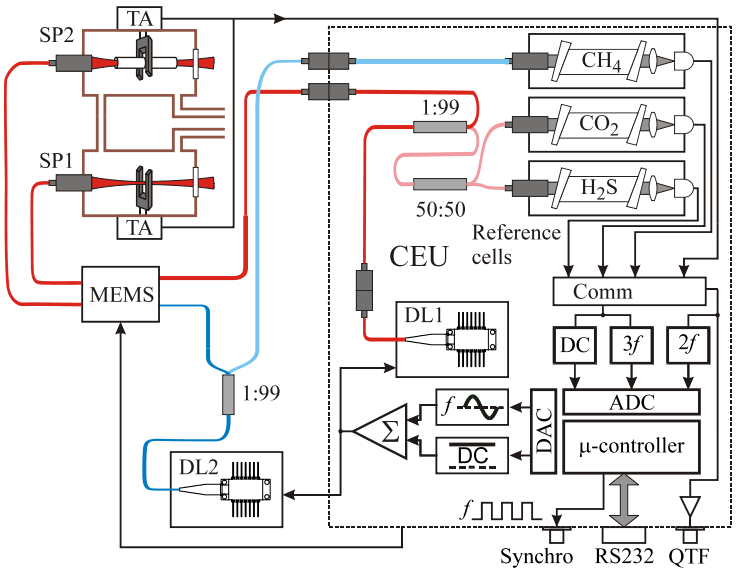

Fig. 2 Schematic of the QEPAS sensor for analyzing concentrations of the three gases. The device also includes temperature, pressure, and relative humidity sensors immersed in the gas stream immediately before the spectrophones, not shown here. *CEU*—control electronics unit; *DL*1, *DL*2—diode lasers; *SP*1—spectrophone without microresonator, *SP*2—spectrophone with microresonator; *TA*—transimpedance amplifier

Table 1 Sensitivity measured in dry and wet N_2 as a trace gas carrier. Wet N_2 contained from 1.1% to 1.4% water vapor by volume. All measurements are performed at atmospheric pressure. Detection bandwidth is 0.785 Hz, corresponding to 1 s interval between readings from the CEU. NE—noise equivalent; NNEA—normalized noise equivalent absorption coefficient in $cm^{-1}\,W/\sqrt{Hz}$

Species	H_2S		CO_2		CH_4	
Carrier	Dry	Wet	Dry	Wet	Dry	Wet
Excitation frequency, cm^{-1}	6320.6		6321.20		6057.09	
Laser power, mW	38.3		37.9		16.0	
NE concentration, ppm	10.1	9.1	270	123	1.5	0.5
NE absorption coeff., cm^{-1}	1.4×10^{-7}	1.2×10^{-7}	2.6×10^{-7}	1.2×10^{-7}	6.4×10^{-7}	2.1×10^{-7}
NNEA	5.8×10^{-9}	5.3×10^{-9}	1.1×10^{-8}	4.0×10^{-9}	1.1×10^{-8}	3.7×10^{-9}

microresonator tubes. The microresonator was formed by two pieces of hypodermic, stainless steel tubing with inner diameter 0.51 mm, outer diameter 0.81 mm, and 4.4 mm long, separated from the QTF by ~30 μm gaps. In order to protect the silver electrodes of the QTF from H_2S, they were electroplated with a 5 μm layer of gold. This shifted the natural frequency of the QTF from 32.8 kHz to 32.2 kHz.

Using an additional spectrophone Sp1 without a microresonator served two purposes. First, it expanded the dynamic range of the sensor. While the linear dynamic range of the QTF itself is extremely wide and sufficient for any practical gas-sensing task, the dynamic range of the digitizing electronics did not allow performing both measurements of the thermal noise of the QTF and a photoacoustic signal produced by 100% CH_4 in the spectrophone with a microresonator. An additional spectrophone with only a QTF expanded the dynamic range ~10 times, which was sufficient for the reported application. A second purpose was to assist in the unambiguous interpretation of our experimental results. A coefficient relating optical absorption in the gas with the electrical response of a spectrophone depends on the speed of sound in the gas, and the dependence is different for two kinds of spectrophones shown in Fig. 1. Therefore, having the information from the two spectrophones helps in the reliable identification of the gas composition.

A 4 × 4 MEMS switch made by combining two 1 × 4 switches (LightBend Mini 1 × 4, Agiltron Inc.) was used to direct any of the two lasers to any of the two spectrophones. The switch was controlled by a parallel 4-bit binary code supplied by a control electronics unit, CEU. As shown in Fig. 3, the CEU incorporated also an electronic switchboard to select signal from one of the spectrophones and from one of the three reference cells. All the three reference cells and the laser DL1 were mounted inside the CEU with 10 × 25 × 25 cm dimensions. As in previous versions [1], the CEU performed the functions of locking the laser wavelength to the selected absorption line, measuring the QTF parameters, and modulating the lasers at half the resonant frequency of the corresponding QTF. To determine the QTF parameters, an electrical, sine wave excitation voltage was applied to it, and the excitation frequency was scanned to find out the QTF natural frequency by measuring the QTF

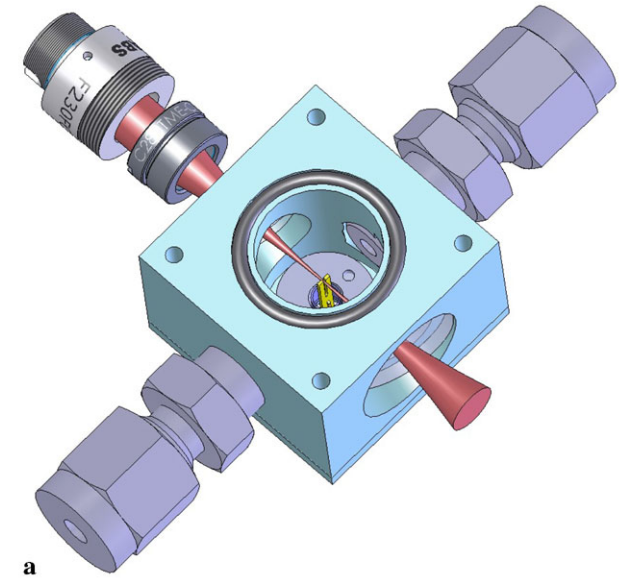

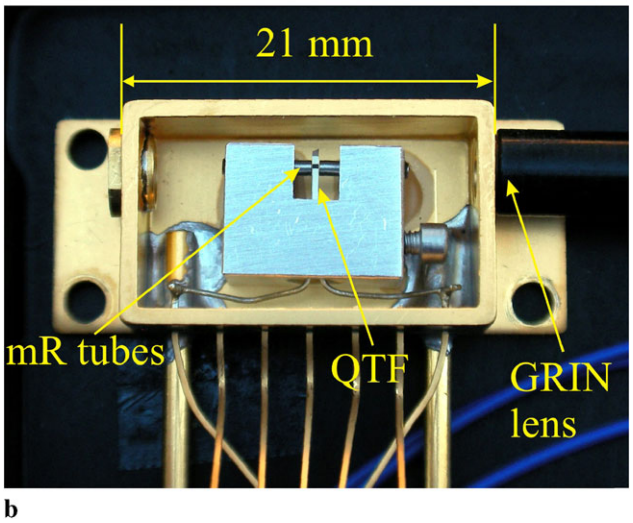

Fig. 3 Sp1—no microresonator (**a**) and Sp2—photo Achray (**b**)

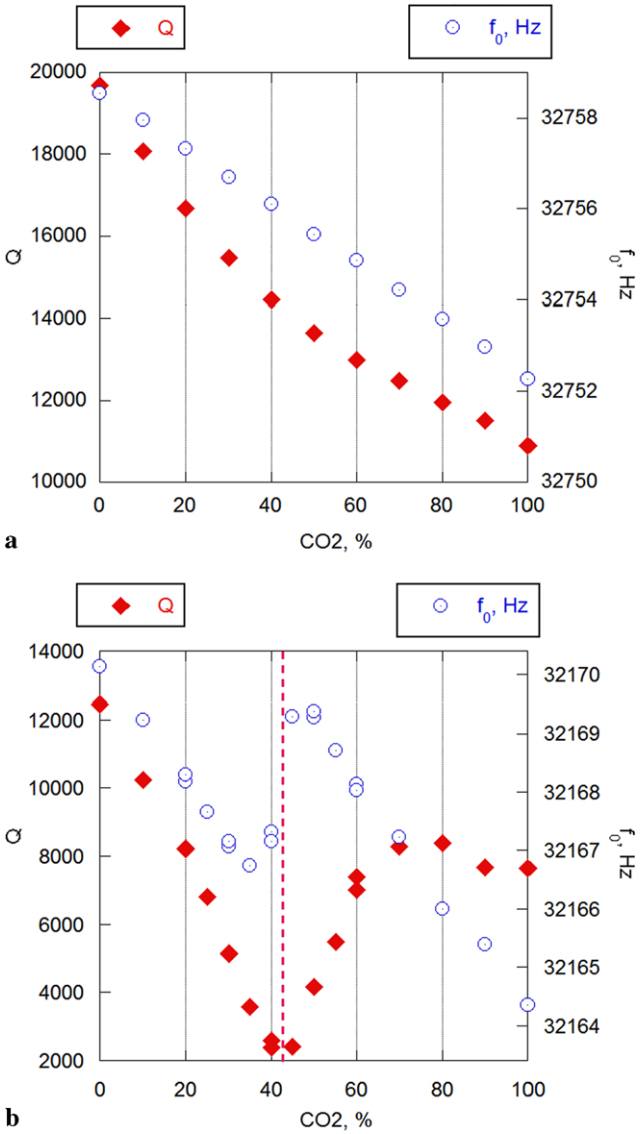

Fig. 4 Q-factor and resonance frequency f_0 of the QTFs as a function of gas mixture: Sp1 (**a**) and Sp2 (**b**)

current. The Q-factor was derived from the QTF ringdown time following a rapid interruption of the excitation voltage.

Up to 10 sets of parameters can be pre-programmed in the CEU, each set including the selection of the laser, the reference cell, and the spectrophone, laser current and temperature, modulation depth, and regulation parameters. The CEU can be programmed to loop through the desired sets of parameters in an autonomous mode. Besides, it can communicate with an external computer through RS232, receiving commands and exchanging data.

3 Results and physical interpretation

Initially the device sensitivity was evaluated in nitrogen as a carrier, using calibrated trace gas sources and more sensitive Sp2. The results are shown in Table 1. They correspond to the detection bandwidth of 0.785 Hz, which is set by the internal CEU digital filters and is applicable when the data are read every 1 s without additional averaging. It can be seen that H_2O has a significant impact on QEPAS sensitivity to CO_2 and CH_4. However, it was determined that methane plays the same role of the V-T relaxation catalyst as H_2O in N_2. Therefore, in gas mixtures containing >5% CH_4 relaxation of both CO_2 and CH_4 is fast enough to satisfy $2\pi f\tau < 1$ condition, and the measured QEPAS signal is not noticeably affected by this factor.

Before performing the gas-sensing measurements in variable carriers, we analyzed the resonant properties of the spectrophones when they were filled with a mixture of CO_2:CH_4 in different proportions. The results are shown in

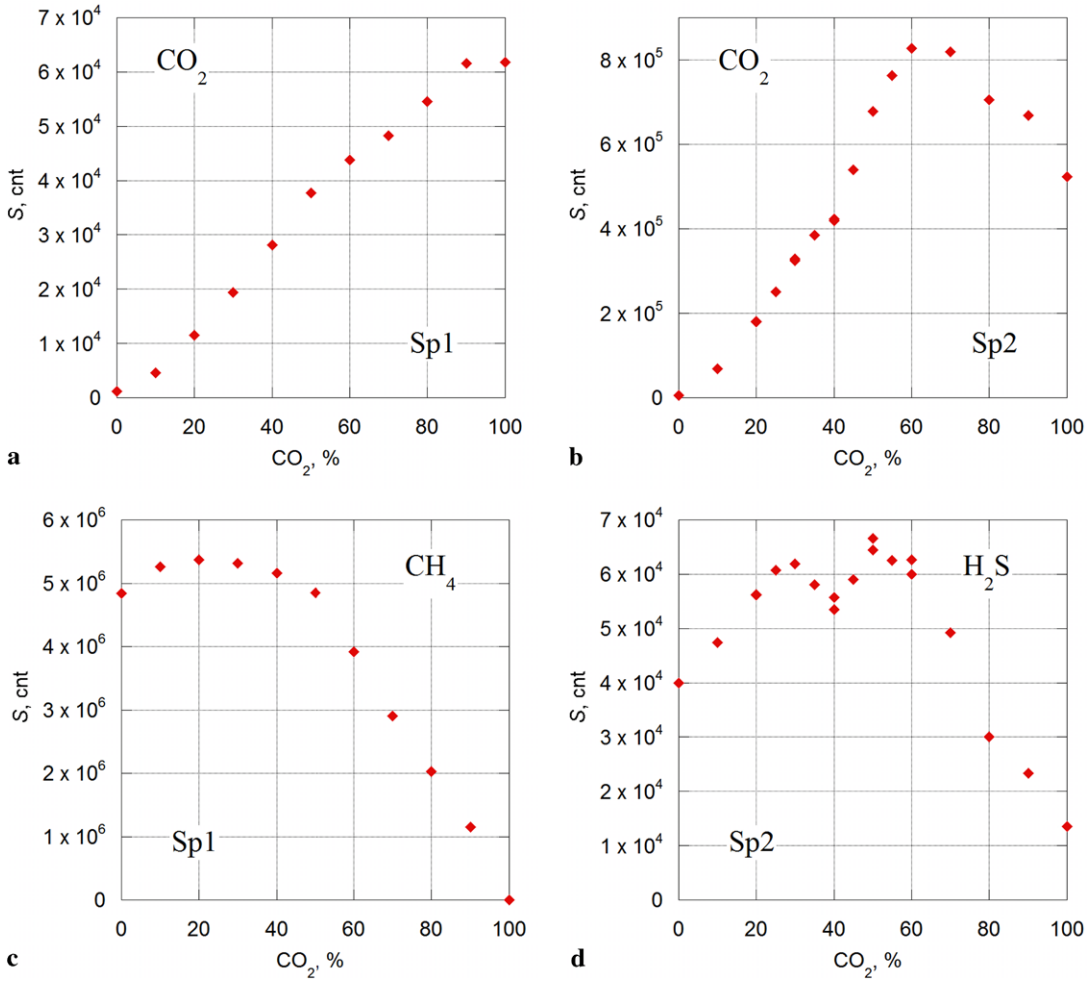

Fig. 5 Raw measurement results. The system saturates at $S = 2^{23} \approx 8.4 \times 10^6$ cnt

Fig. 4. The Sp1 shows a smooth $Q(C)$ and linear $f_0(C)$ dependences, where C is a fraction of CO_2 in the gas mixture and f_0 is the resonant frequency of the QTF. The Sp2 shows a minimum in $Q(C)$ corresponding to the fastest growth of $f_0(C)$ at $C = 42\%$. This feature appears when the natural frequency of the microresonator coincides with the natural frequency of the QTF. The speed of sound in the CO_2:CH_4 mixture at $C = 42\%$ is 337 m/s (calculated from the gas parameters and verified by direct measurements), close to the speed of sound in air, which confirms the correct Sp2 design.

Next, the photoacoustic response of the sensor to mixtures containing 0.5% H_2S and variable amounts of CH_4 and CO_2 was studied. Because of the weak H_2S signal and the need to measure trace concentrations of this species, only more sensitive Sp2 was used for H_2S measurements. High concentrations of CH_4 caused the signal from Sp2 to saturate the electronics, and therefore only Sp1 was used for the CH_4 measurements. For CO_2, where a weak $3\nu_3 + \nu_1$ band is excited but the concentration is high, signals from both spectrophones were recorded. The results of the measurements are shown in Fig. 5. The signal S is expressed in the internal ADC counts (cnt), which can be directly read from the CEU RS232 port. Each point was a result of averaging 10–20 individual measurements, and the peak-to-peak noise of a single measurement is ~1000 cnt. Thus, errors in the plots were primarily determined by flow controllers in the gas dilution system and did not exceed 1% (horizontal scale). We verified that off-the-trend point at zero CH_4 concentration in plot (Fig. 5a) is correct and related to the relaxation dynamics (CH_4 presence increasing the relaxation rate of excited CO_2). Physically, 1 cnt $= 6.67 \times 10^{-16}$ A of QTF rms current. The following factors impact the QEPAS signal:

- The analyte concentration.
- Cross-talk between the partially overlapping lines of CO_2 and H_2S. In this application, the CO_2 concentrations are high and the H_2S concentrations are low. Therefore, a practically important effect is a negative offset to the H_2S signal created by high CO_2 concentrations, which will be discussed below.

- Vibrational-to-translational (V-T) energy transfer rates and pathways. As will be shown below, high concentrations of CO_2 will partially quench the QEPAS signal from H_2S, apart from the negative signal offset mentioned above.
- Carrier gas dependent QTF quality factor, especially in Sp2.
- Scaling factor $(\gamma - 1)$ in the source term of the equation governing the generation of the photoacoustic signal [11]. This factor changes from 0.289 for pure CO_2 to 0.304 for pure CH_4, and we neglect this 5% change.
- Speed of sound, affecting the sensitivity of both spectrophones but in a different way. In Sp1, the sensitivity is changing because of the geometric stretching of the function describing the acoustic field distribution [11] as shown in Fig. 6a. In Sp2, the main factor affecting the sensitivity is detuning between acoustic resonance of the microresonator and mechanical resonance of the QTF (Fig. 6b).

The resonant frequency of the acoustic gas resonator is proportional to the speed of sound v_s. For calculating v_s in the gas mixture, we can use the usual equation

$$v_s = \sqrt{\gamma \frac{RT}{M}} \tag{1}$$

where $\gamma = c_p/c_v$ is the adiabatic coefficient, $R = 8.31$ J/(Mol K) is the gas constant, T is the absolute temperature and M is the molar mass. For a mixture of two gases, M, c_p and c_v are calculated as weighted mean values according to the volume gas fractions in the mixture. We took $c_p(CH_4) = 35.52$ J/(Mol K), $c_v(CH_4) = 27.2$ J/(Mol K), $c_p(CO_2) = 37.136$ J/(Mol K), and $c_v(CO_2) = 28.82$ J/(Mol K) using the data from Ref. [12]. We also performed direct measurements of the speed of sound in a tube; the setup is shown in Fig. 7. A hypodermic stainless steel tube $l = 26$ cm long with an outer diameter of 1.65 mm and inner diameter 1.19 mm was used as a sound guide. Theory predicts that the speed of sound in a tube with rigid walls is equal to the speed of sound in the open space. Sound was generated by a small speaker in $f = 27$–35 kHz frequency range and detected by two miniature MEMS microphones (Knowles Acoustics SPM0404HE5H-PB) with a 0.84 mm diameter acoustic port. The phase difference φ between the two microphones was measured as a function of speaker frequency, and the speed of sound was found using the equation:

$$v_s = 2\pi l \left(\frac{d\varphi}{df}\right)^{-1}. \tag{2}$$

The v_s values calculated using (1) and determined from experimental data using (2) are in a good agreement, as shown in Fig. 8.

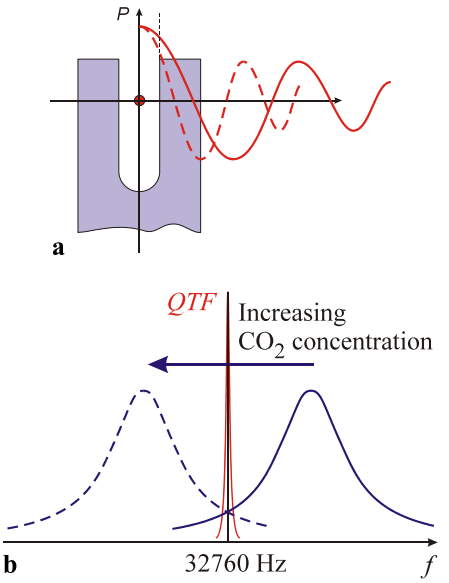

Fig. 6 Speed of sound effect on the QEPAS signal for a spectrophone without microresonator (**a**) and with microresonator (**b**). In both cases the *dashed line* corresponds to higher CO_2 concentration, meaning lower speed of sound, shorter sound wavelength, and lower resonant frequency of an acoustic resonator. The *curves* in (**a**) represent a snapshot of the acoustic pressure field

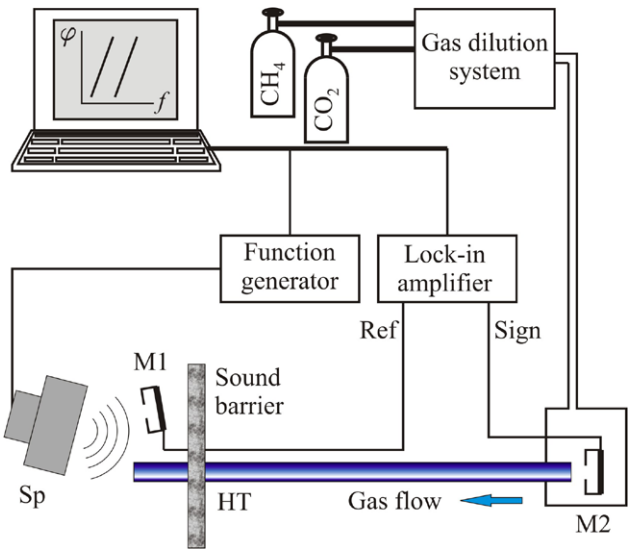

Fig. 7 Measuring the speed of sound. *M1*, *M2*—miniature microphones, *Sp*—speaker, *HT*—hypodermic tube. Lock-in amplifier measures the phase difference between two microphones while the speaker frequency is scanned. The slope of $\varphi(f)$ determines the speed of sound

For a better understanding of the data, the signal from Sp2 can be divided by Q of the QTF, which is directly measured by the CEU by means of the electrical excitation of the QTF. The result reflects the magnitude of the acoustic pressure acting on the QTF and manifests the resonant properties of the microresonator. If we assume that the effect of the microresonator resonance shift with the

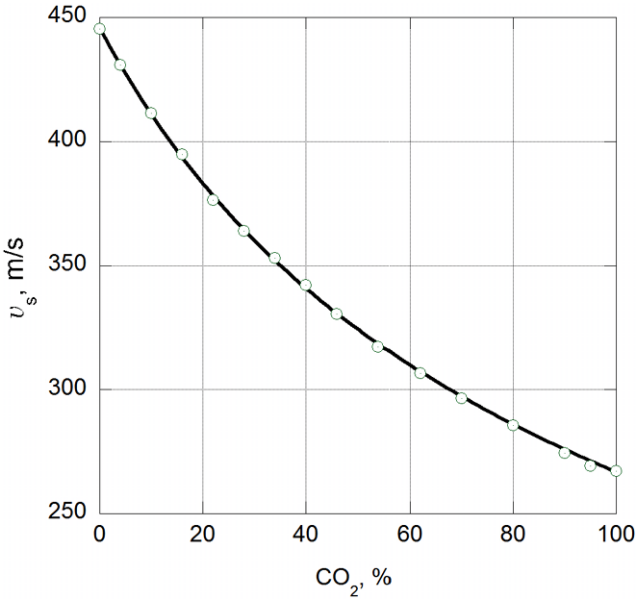

Fig. 8 Speed of sound in a CO_2:CH_4 mixture, calculated (*line*) and measured (*circles*)

changing speed of sound governs the signal, then this signal squared and plotted as a function of the speed of sound must follow Lorentzian curve. Such a fit is shown in Fig. 9 for H_2S and CO_2 signals, normalized to H_2S and CO_2 concentrations, respectively. Both signals behave similarly and yield almost the same fit parameters. The maximum is located at $v_s = 336$ m/s ($C = 43\%$), in agreement with $Q(C)$ from Fig. 4. The peak position also agrees with the observed phase of the photoacoustic signals (Fig. 12). The width of the tuning curve yields the quality factor of the microresonator $Q_{mR} = 17$.

The overlapping absorption bands of H_2S and CO_2 make it impossible to find a perfectly isolated, interference-free H_2S line at atmospheric pressure. In Fig. 10 the target H_2S line is shown together with the closest CO_2 line, which creates a *negative* offset to the H_2S QEPAS signal. Coinciding phases of H_2S and CO_2 signals make it easier to compensate for the CO_2 interference at the H_2S wavelength. We performed a set of measurements of varying H_2S concentrations in CO_2:CH_4 mixtures of different composition. They prove that this negative offset signal is independent of H_2S concentration. An example of such a measurement is shown in Fig. 11. The laser wavelength was locked to H_2S absorption line using the reference cell, and the QEPAS signal was detected. Similar measurements were performed with other mixing ratios of CO_2:CH_4. It was found out that the negative offset to the H_2S signal created by the CO_2 line wings is 0.011 of the peak CO_2 signal.

Phases of H_2S and CO_2 signals practically coincide (Fig. 12), pointing to no essential V-T relaxation delay. Therefore we conclude that CO_2 relaxation is promoted by

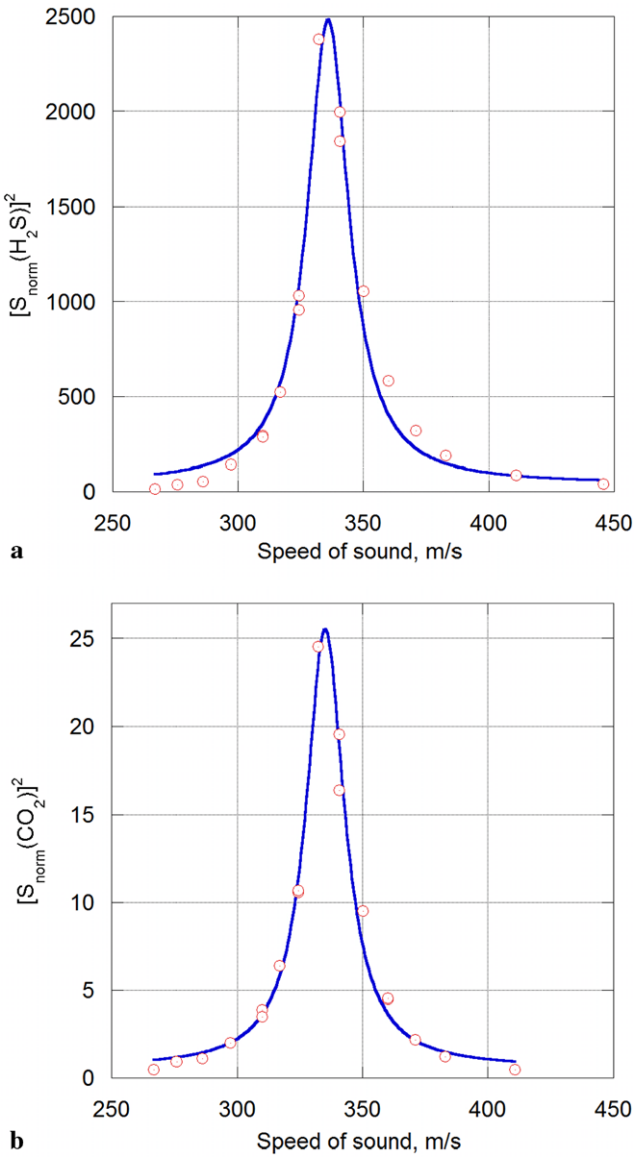

Fig. 9 Square of the normalized to Q QEPAS signal fitted by a Lorentzian curve: H_2S (**a**) and CO_2 (**b**)

the presence of CH_4. This explains a somewhat out-of-the-trend position of the $C = 100\%$ (no CH_4) point in Fig. 5a and Fig. 12b plots. CO_2, however, has an impact on the V-T relaxation of H_2S, branching part of the initial excitation into slowly relaxing intramolecular states and thus removing this portion of energy from producing the photoacoustic signal. It can be seen if we plot the ratio of H_2S to CO_2 signals from Sp2 (Fig. 13). At low CO_2 concentrations the device is 14.2 times more sensitive to H_2S than to CO_2 because of the stronger absorption line of H_2S, while at 100% CO_2 this number drops to 7.4. The calibration will hold true as soon as H_2S concentration is low, so that the rate of collisions with the carrier gas molecules is much higher then self-collisions. Since the linear fit in Fig. 13 does not rep-

resent a physical model, we estimate its validity to be ∼5% based on the scattering of the points.

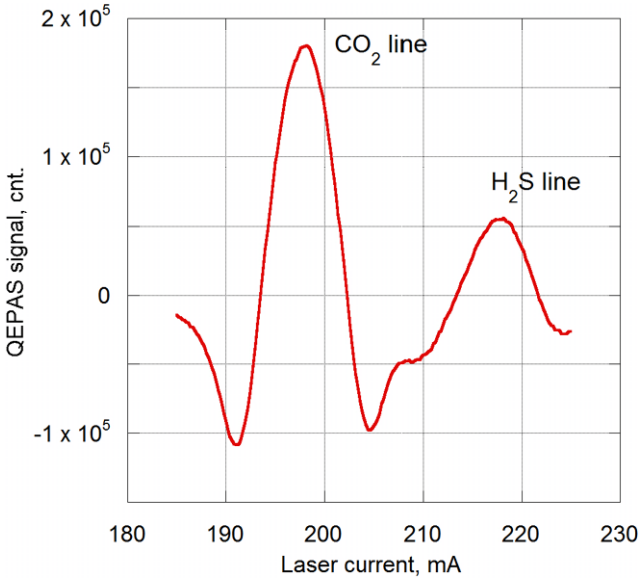

Fig. 10 QEPAS signal ($2f$ wavelength modulation) from Sp2 when the laser current is scanned. The H_2S line at 6320.6 cm^{-1} and the CO_2 line at 6321.20 cm^{-1}, both used for the concentration analysis, partially overlap at atmospheric pressure. The gas mixture contains 20% CO_2, ∼80% CH_4, and 0.5% H_2S

In Fig. 14 summarizes the observed dependences of H_2S QEPAS signal and QTF properties on the CO_2 content in a CO_2:CH_4 mixture and presents them as a minimum detectable concentration. It is defined as the concentration producing QEPAS signal with a RMS equal to the thermal noise of the QTF in a 0.785 Hz band. This plot does not take into

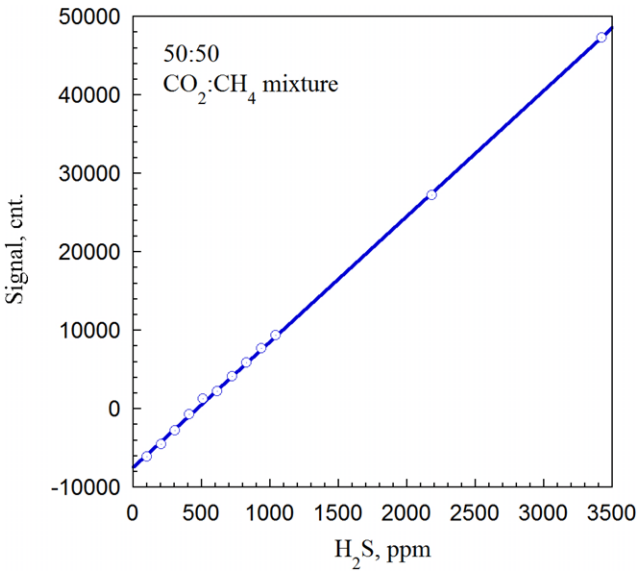

Fig. 11 QEPAS signal from H_2S at low concentrations

Fig. 12 Phase of the photoacoustic signals from Sp2

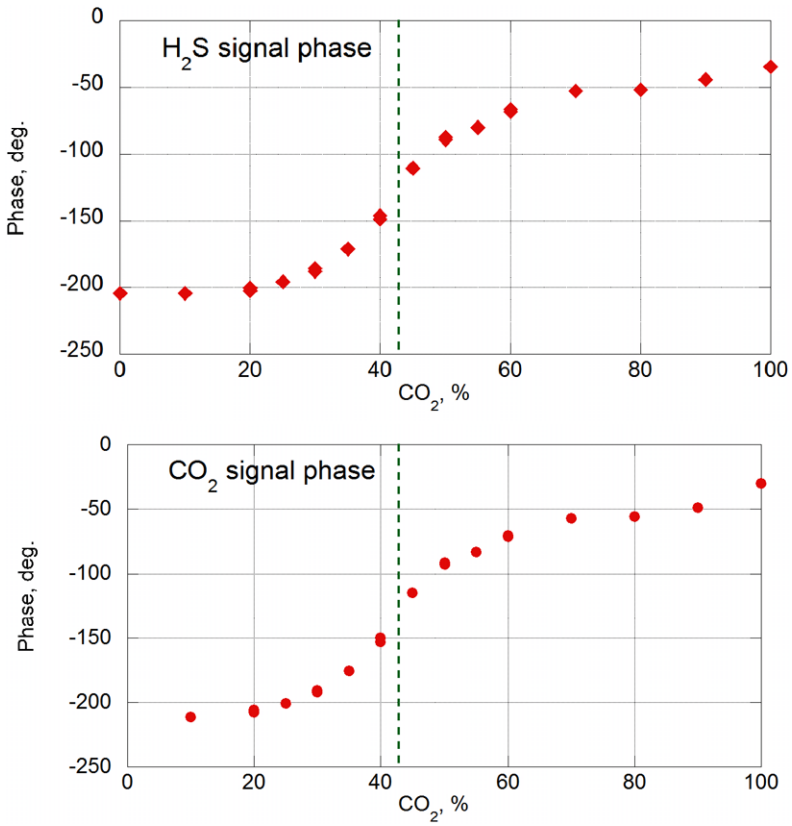

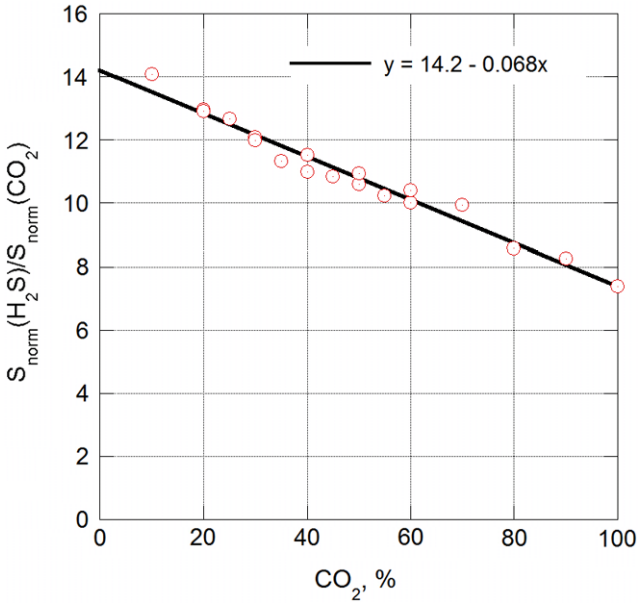

Fig. 13 Ratio of H_2S and CO_2 QEPAS signals, both normalized to their respective concentrations

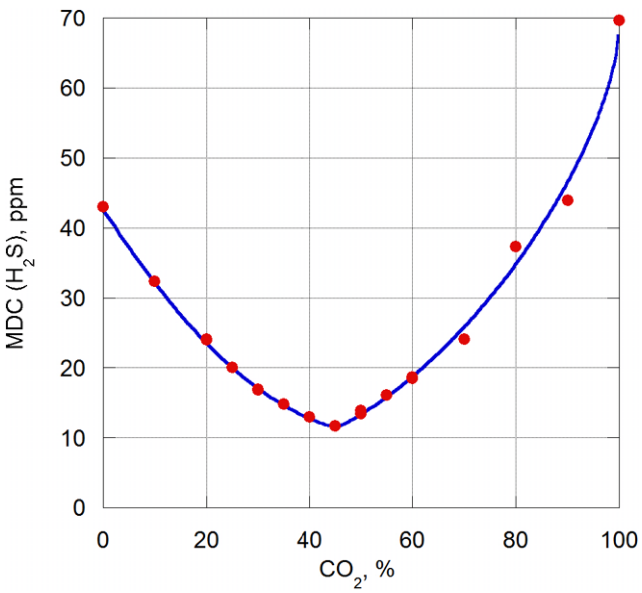

Fig. 14 Minimum detectable concentration of H_2S defined as the concentration producing QEPAS signal with rms equal to the thermal noise of the QTF in 0.785 Hz band. The *blue curve* is a trend guide

account uncertainties in determining the CO_2 concentration based on data from Sp1.

For a better understanding of CO_2 and CH_4 signals from Sp1, a number of normalizations should be performed. First, QEPAS signals for the spectrophone type depicted in Fig. 1b depend on the speed of sound, as explained in Fig. 6a. Using the $v_s(C)$ dependence from Fig. 8 and the model described in [11], N. Petra calculated the correction factor as a function of CO_2 concentration. This factor is shown in Fig. 15 as a

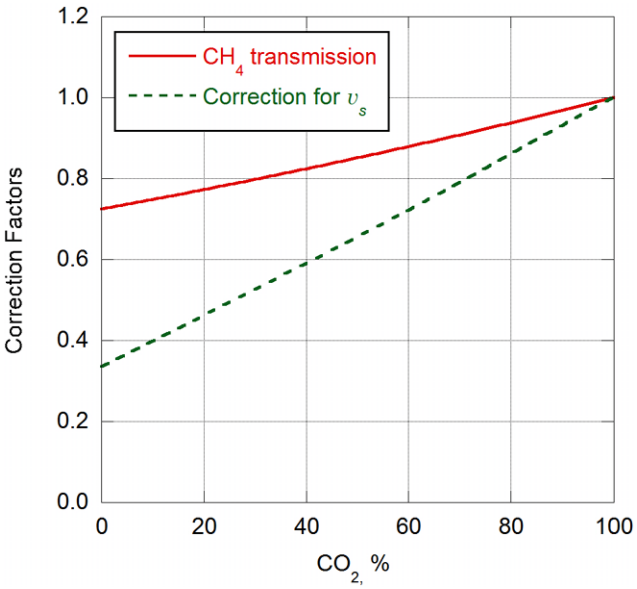

Fig. 15 Correction factors for QEPAS signals from Sp1

dashed line, normalized to be 1 at 100% CO_2 concentration. Second, the attenuation of optical radiation in its 0.92 cm long path from the window to the QTF in Sp1 cannot be neglected for the CH_4 line. The corresponding calculated optical transmission is shown in Fig. 15 as a solid line.

The CO_2 and CH_4 QEPAS signals from Sp1 normalized to these correction factors and also to Q and CO_2 or CH_4 concentration, respectively, are shown in Fig. 16a. The maximum observed at $C = 50\%$ most likely results from an accidental acoustic resonance in the Sp1 enclosure. This is confirmed by the phase data in Fig. 16b. The phase change rate is highest at $C = 50\%$, which is an indication of crossing the resonance. The phase dependence on CO_2 concentration is similar for CO_2 and CH_4 signals, except for the almost constant shift. This shift is due to the different laser drivers and different laser designs (lasers manufactured by different companies), causing a different phase shift between the control voltage and the wavelength modulation of the laser. The rapid phase change for the CO_2 signal at $C = 100\%$ is caused by the slower V-T relaxation of the excited CO_2 when CH_4 is absent. Apart from that, there is no dramatic difference in V-T relaxation rates of CO_2 and CH_4, as indicated by the phase and amplitude data in Fig. 16.

4 Practical procedures for concentration analysis

The Lorentzian fit in Fig. 9 proofs the physical model of Sp2 operation and allows the evaluation of the Q-factor of the acoustic microresonator, and it is helpful in designing next versions of spectrophones. However, the fit is not sufficiently close for quantitative analysis of the gas mixture. Therefore, a different approach was developed for the data

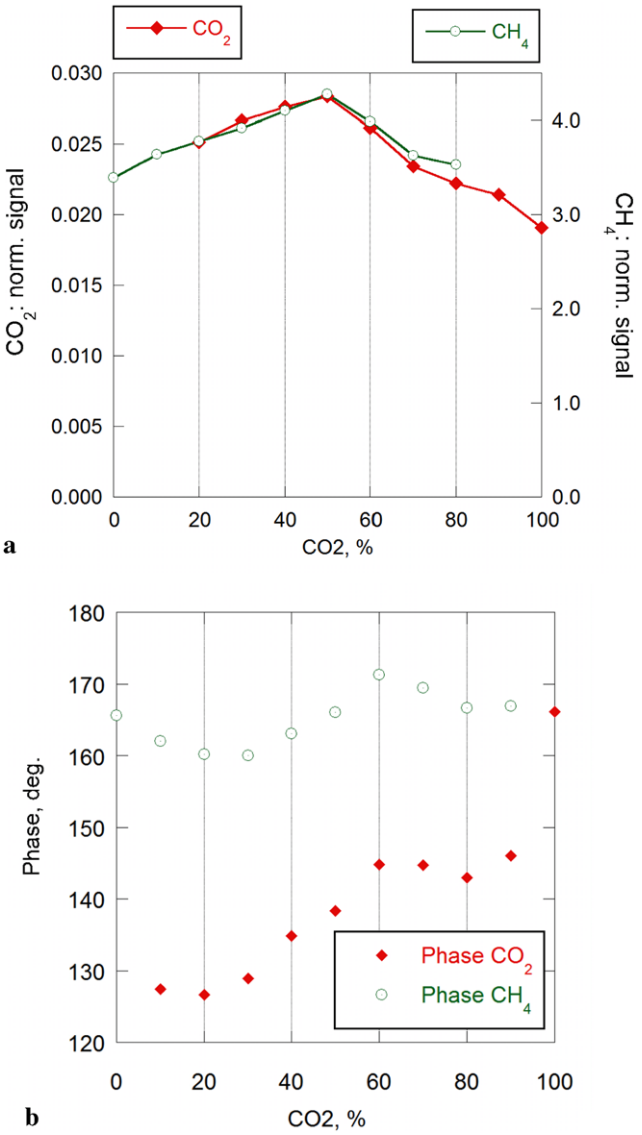

Fig. 16 Corrected signals from Sp1 (**a**) and phase of these signals (**b**)

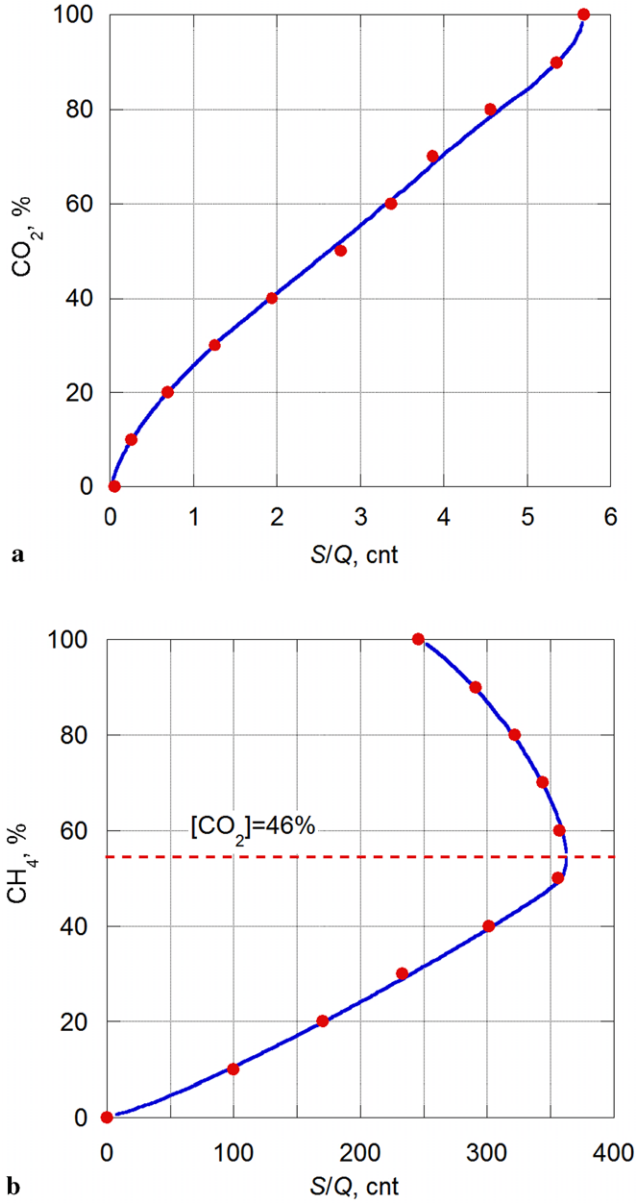

Fig. 17 A curve for determining CO_2 concentration based on QEPAS signal from Sp1 (**a**) and a similar curve for CH_4 (**b**). The *blue curve* is a trend guide

analysis, based on the fact that in this application the CO_2 is expected to be present at least at several percent concentration levels. In our data analysis we avoided using quantities which directly depend on the physical properties of the QTF, such as its Q and f_0, because these properties can change when the QTF is contaminated. Instead, S/Q was used, which depends only on the acoustic pressure acting on the QTF and on the electromechanical coefficient of the QTF.

The procedure we apply for the QEPAS data analysis consists of three steps:

1. Use $S(CO_2)/Q$ data from Sp1 to determine the concentration of CO_2 by means of the calibration curve in Fig. 17a derived from Fig. 4a and Fig. 5a data.
2. Based on the CO_2 concentration, determine the branch on the Fig. 17b calibration curve and determine the concentration of CH_4 using $S(CH_4)/Q$ data from Sp1.
3. Use $S(CO_2)$ data from Sp2 as the sensitivity calibration for Sp2. This approach eliminates the need to know exactly the resonant curve of the microresonator (Fig. 9), which depends on the gas composition and temperature. Knowing $S(CO_2)$, the CO_2 concentration, and $S(H_2S)$, the H_2S concentration can be calculated using the Fig. 13 plot. The following equation gives the concentration

[H_2S] expressed as a function of the QEPAS signals from Sp2 and [CO_2] concentration:

$$[H_2S] = \frac{S(H_2S) + 0.011S(CO_2)}{\{14.2 - 0.068[CO_2]\} \times \frac{S(CO_2)}{[CO_2]}}. \quad (3)$$

Summing in the numerator takes care of the spectral overlapping of the two absorption lines; the denominator uses calibration curve of Fig. 13, and the ratio of the CO_2 signal to its concentration represents the resonant curve. The numerical coefficients do not have direct physical meaning.

If the carrier gas contains large quantities (percents, at least) of other components besides CO_2 and CH_4, it may reduce the accuracy of the result because of the change of the speed of sound and hence the change of the dashed curve from Fig. 15. It is assumed that the real gas in the outer layers of flexible oil risers may contain H_2 and H_2O vapor. Based on the results of this work, we propose to add a speed of sound measurement module to the sensor. The architecture of such a module will be similar to the setup shown in Fig. 7. For compactness, the tube can be coiled. The water vapor concentration cannot exceed the saturated vapor pressure and therefore will not significantly impact v_s. Therefore, information about v_s combined with temperature data will not only improve the accuracy of H_2S, CH_4, and CO_2 concentration measurements but also provide indirect information about the H_2 concentration. Another future modification is to introduce a QTF signal preamplifier with a switchable amplification coefficient, which will extend the dynamic range of each spectrophone.

5 Conclusions

Application of QEPAS to chemical analysis of multi-component gas mixtures is a complicated task because of several involved physical processes linked to the speed of sound, molecular relaxation dynamics, and overlapping of absorption lines. Therefore, a detailed study is needed for each particular case of such application. The reported work provides an example of such a study and can serve as a guide to developing the data-analysis approaches in similar cases. Regardless of the complexity of the involved phenomena, it was possible to derive a simple data-analysis algorithm that provides sufficient accuracy of the results. The developed sensor has small sensing modules (spectrophones) and a wide dynamic range, allowing measuring both H_2S at ppm levels and CH_4 and CO_2 at up to 100% levels.

Acknowledgements Authors thank Noemi Petra for calculating the QTF sensitivity as a function of the speed of sound. The Rice University Laser Science Group acknowledges financial support from NKT Flexibles, the National Science foundation ERC MIRTHE award and a grant C-0586 from The Welch Foundation.

References

1. A.A. Kosterev, F.K. Tittel, D.V. Serebryakov, A.L. Malinovsky, I.V. Morozov, Rev. Sci. Instrum. **76**, 043105 (2005)
2. D.V. Serebryakov, I.V. Morozov, A.A. Kosterev, V.S. Letokhov, Quantum Elec. **40**, 167 (2010)
3. A. Elia, P.M. Lugara, C.D. Franco, V. Spagnolo, Sensors **9**, 9616 (2009)
4. K. Liu, J. Li, L. Wang, T. Tan, W. Zhang, X. Gao, W. Chen, F.K. Tittel, Appl. Phys. B **94**, 527 (2009)
5. K. Liu, H. Yi, A.A. Kosterev, W. Chen, L. Dong, L. Wang, T. Tan, W. Zhang, F.K. Tittel, X. Gao, Rev. Sci. Instr. (to appear Sept. 2010)
6. L. Dong, A.A. Kosterev, D. Thomazy, F.K. Tittel, Appl. Phys. B **100**, 627 (2010)
7. R. Lewicki, A.A. Kosterev, D. Thomazy, L. Gong, R. Griffin, T. Day, F.K. Tittel, *LTuD2, Laser Applications to Chemical, Security and Environmental Analysis (LACSEA)*, January 31–February 3, 2010, San Diego, CA, USA
8. V. Spagnolo, A.A. Kosterev, L. Dong, R. Lewicki, F.K. Tittel, Appl. Phys. B **100**, 125 (2010)
9. R.F. Curl, F. Capasso, C. Gmachl, A.A. Kosterev, B. McManus, R. Lewicki, M. Pusharsky, G. Wysocki, F.K. Tittel, Chem. Phys. Lett. **487**, 1–18 (2010)
10. A. A Kosterev, F.K. Tittel, G. Bearman, SAE Int. J. Aerosp. **1**, 331 (2008)
11. N. Petra, J. Zweck, A.A. Kosterev, S.E. Minkoff, D. Thomazy, Appl. Phys. B **94**, 673 (2009)
12. www.engineeringtoolbox.com